MIT Libraries | DSpace@MIT

MIT Open Access Articles

High-Speed Vapor Transport Deposition of Perovskite Thin Films

The MIT Faculty has made this article openly available. ***Please share*** how this access benefits you. Your story matters.

Citation: Hoerantner, Maximilian et al. "High-Speed Vapor Transport Deposition of Perovskite Thin Films." ACS Applied Materials & Interfaces 11, 36 (August 2019): 32928-32936 © 2019 American Chemical Society

As Published: http://dx.doi.org/10.1021/acsami.9b07651

Publisher: American Chemical Society (ACS)

Persistent URL: https://hdl.handle.net/1721.1/122275

Version: Final published version: final published article, as it appeared in a journal, conference proceedings, or other formally published context

Terms of use: Creative Commons Attribution-NonCommercial-NoDerivs License

Massachusetts Institute of Technology

This is an open access article published under a Creative Commons Non-Commercial No Derivative Works (CC-BY-NC-ND) Attribution License, which permits copying and redistribution of the article, and creation of adaptations, all for non-commercial purposes.

ACS APPLIED MATERIALS & INTERFACES

Research Article

Cite This: ACS Appl. Mater. Interfaces 2019, 11, 32928−32936

www.acsami.org

High-Speed Vapor Transport Deposition of Perovskite Thin Films

Maximilian T. Hoerantner,*[,†] Ella L. Wassweiler,[†] Haomiao Zhang,[‡] Anurag Panda,[†] Michel Nasilowski,[§] Anna Osherov,[†] Richard Swartwout,[†] Aidan E. Driscoll,[†] Nicole S. Moody,[§] Moungi G. Bawendi,[§] Klavs F. Jensen,[‡] and Vladimir Bulović*[,†]

[†]Department of Electrical Engineering and Computer Science Department, [‡]Department of Chemical Engineering, and [§]Department of Chemistry, Massachusetts Institute of Technology, 77 Massachusetts Avenue, Cambridge, Massachusetts 02139, United States

Supporting Information

ABSTRACT: Intensive research of hybrid metal-halide perovskite materials for use as photoactive materials has resulted in an unmatched increase in the power conversion efficiency of perovskite photovoltaics (PVs) over the last couple of years. Now that lab-fabricated perovskite devices rival the efficiency of silicon PVs, the next challenge of scalable mass manufacturing of large perovskite PV panels remains to be solved. For that purpose, it is still unclear which manufacturing method will provide the lowest processing cost and highest quality solar cells. Vapor deposition has been proven to work well for perovskites as a controllable and repeatable thin-film deposition technique but with processing speeds currently too slow to adequately lower the production costs. Addressing this challenge, in the present work, we demonstrate a high-speed vapor transport processing technique in a custom-built reactor that produces high-quality perovskite films with unprecedented deposition speed exceeding 1 nm/s, over 10× faster than previous vapor deposition demonstrations. We show that the semiconducting perovskite films produced with this method have excellent crystallinity and optoelectronic properties with 10 ns charge carrier lifetime, enabling us to fabricate the first photovoltaic devices made by perovskite vapor transport deposition. Our experiments are guided by computational fluid dynamics simulations that also predict that this technique could lead to deposition rates on the order of micrometers per second. This, in turn, could enable cost-effective scalable manufacturing of the perovskite-based solar technologies.

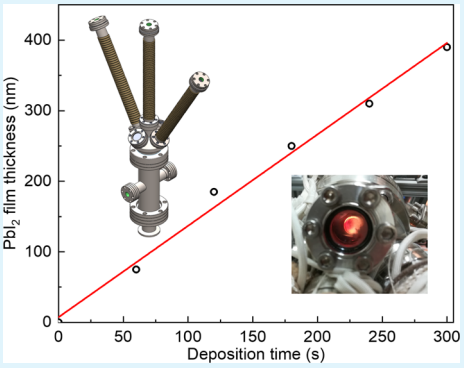

KEYWORDS: *solar cells, perovskite, thin-film, vapor deposition, manufacturing, fluid dynamics*

INTRODUCTION

The latest report showing hybrid metal-halide perovskite solar cells with power conversion efficiency (PCE) exceeding 23% for longer than 1000 h[1] is a remarkable demonstration of one of the presently most promising emerging energy technologies. In this record demonstration, as well as in other recent reports of the highest-PCE perovskite solar cells, the photoactive layers of the devices were fabricated via spin-coating method, which, unfortunately, is not scalable, as would be needed for their mass production. Solution processing brings a number of challenges inherent in the solvent drying kinetics, which make it difficult to independently control film formation and crystallization to achieve the desired film quality, especially over large areas:[2] The nonuniformity of solution-coated films can introduce macroscopic defects that can act as shunt pathways, nonactive areas, and avenues for moisture and metal ingress, compromising device stability.[3,4] Solution processing also introduces fabrication challenges for more advanced stacked multilayer perovskite solar cells,[5,6] as solvents used in one layer need to be compatible with deposition on top of all of the underlying layers. Above all, standard solvents used in perovskite film processing are often toxic, resulting in hazardous solvent waste on a production line and making it to either replace them or eliminate them, as we do in the present work where we demonstrate solvent-free vapor deposition.

State-of-the-art vapor-deposited perovskite solar cells, fabricated via vacuum thermal evaporation (VTE),[7,8] have exceeded 20% efficiency.[9] However, this record demonstration relied on the photoactive layer deposition at low operating pressures (10^{-6} Torr), requiring ultra-high-vacuum equipment and long pump-down times that could be limiting manufacturing throughput. The speed of production influences heavily the manufacturing cost of the solar module. As the price for currently sold photovoltaics (PV) modules is well below 1 USD/W_p, the deposition speed needs to be at values higher than currently demonstrated VTE rates of Å/s.[9−11] Additionally, the relatively low material utilization efficiency of <50% increases both material cost per watt and chamber cleaning requirements.[12] Since the evaporation rate varies exponentially

Received: May 23, 2019
Accepted: August 16, 2019
Published: August 16, 2019

Downloaded via MASSACHUSETTS INST OF TECHNOLOGY on September 20, 2019 at 14:22:04 (UTC).
See https://pubs.acs.org/sharingguidelines for options on how to legitimately share published articles.

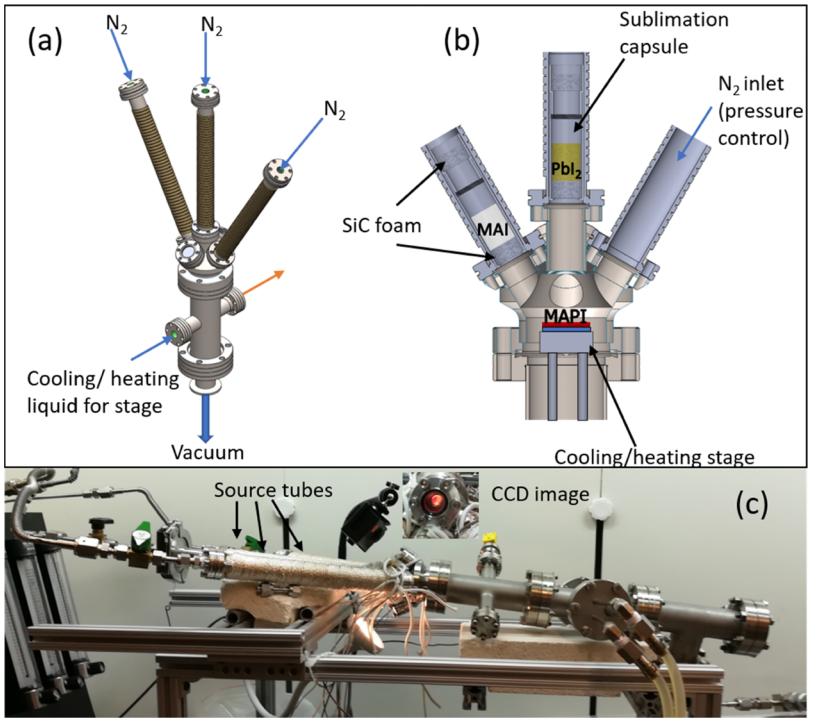

Figure 1. Three-dimensional drawing in perspective (a), 3D drawing of the detailed cross-sectional design (b), and the photograph (c) of the horizontally positioned multisource VTD tool.

with and can only be controlled by the source temperature,[13] precise optimization of multiple co-deposited precursors, as needed for perovskite film deposition, would be difficult to control, and the needed high deposition rates would be limited by the relatively low decomposition temperature of the material.

Many of these limitations and drawbacks could be overcome with another vapor-based process known as vapor transport deposition (VTD), which operates under minimal low-pressure conditions. VTD relies on a transport carrier gas to carry sublimated material vapors from the source to the target substrate, not requiring a chemical reaction of the materials in the vapor phase. VTD has been used commercially to deposit high-quality CdTe films for solar applications at high rates (≥500 nm/s).[14,15] In the field of organic semiconducting materials, a similar process named "organic vapor phase deposition" (OVPD) has been developed, in which organic films are deposited from evaporated organic small molecules delivered by a gas stream through a heated apparatus onto a substrate.[16] It has been demonstrated that this process can be operated at five orders of magnitude higher pressure as compared to thermal evaporation, which is not only saving costs but allows to independently control the deposition rate from temperature by controlling the gas flow rate and pressure. This inherently leads to better control over the morphology of the grown thin films, hence allowing for tuning of material properties.[17−19]

In the field of perovskite solar cells, chemical vapor deposition processes in tube furnaces have been used to convert solution-deposited or thermally evaporated lead halide (PbI_2 or $PbCl_2$) films into perovskites by exposing them to vapor-transported methylammonium iodide (MAI) or formamidinium iodide.[20−22] A similar result was reported by combined chemical vapor deposition of MAI and PbI_2 in the same vacuum tube.[23] The demonstrated results of high-quality perovskite films over large areas prove that vapor-based scaling methods represent a promising route toward forming scalable perovskite solar cells. However, these first demonstrations of precursor depositions and conversion to perovskite films in tube furnaces were unable to exceed the deposition rates of conventional thermal evaporation-based deposition demonstrations, which are inferior to solution-based methods.

Here, we report on the development of a novel method for depositing perovskite thin films with unprecedented high throughput. Our solvent-free process is based on vapor transport deposition with customized adaptations for specific perovskite requirements. We designed dedicated material sublimation sources for the precursor materials that are transported and guided in the vapor state by the individually controlled carrier gas flow toward a temperature-controlled substrate. The fully vapor-deposited perovskite thin films are formed by combining multiple precursors in an alloyed polycrystalline film. We show that perovskite VTD requires pressures not lower than 10 Torr, achievable with simple pumping and chamber equipment. This reduces capital expenditures substantially compared to high-vacuum thermal evaporation. At these pressures, precursor molecules are randomly distributed in the carrier gas, combined with precisely controlled flow, this allows for highly uniform film deposition with high material utilization. VTD decouples evaporation and condensation, allowing orders-of-magnitude higher deposition rates without decomposing the materials.

Accurate compositional control can enable precise stoichiometric deposition of multiple compounds, which, in turn, permits the fabrication of the multicomponent perovskite films. Crystallization conditions can be fine-tuned by varying the substrate temperature and deposition pressure, allowing control of the film morphology and defect densities, a key requirement for making efficient and stable devices, hence,

DOI: 10.1021/acsami.9b07651
ACS Appl. Mater. Interfaces 2019, 11, 32928−32936

providing a path to a scalable production of perovskite-based photovoltaics.

RESULTS AND DISCUSSION

We developed a multisource VTD system that integrates temperature and material control with the gas flow (Figure 1a), using nitrogen as the carrier gas. The nitrogen gas is first heated by passing it through heated tubes that are sufficiently long to ensure uniform gas temperature, and then it flows through the equally heated vaporization zones containing the precursor materials, where they get sublimated into the vapor phase and then carried by the transport gas toward a temperature-controlled substrate. The sublimation itself consumes energy, which could lead to a cooling of the system. However, the amount of material being vaporized is low enough that we can assume no influence on the gas flow. The magnified cross-section of the diagram in Figure 1b illustrates the inner components of the VTD system. The custom-made capsules within the source tubes contain the source material, which is capped by two silicon carbide (SiC) foam filters. The capsules with foam filters can be easily extracted and cleaned for optimal uncontaminated operation. The lower filter is used to prevent the solid materials from escaping the source tube, whereas the upper filter ensures uniform gas flow and temperature distribution of the transport gas within the capsule. A temperature-controlled liquid is circulated through the substrate stage to allow for precise control of the substrate surface temperature, which is critical in the control of the crystallinity of deposited films. We loaded the middle source tube with PbI_2 and the outer source tubes with CH_3NH_3I (MAI), which during the deposition process results in the formation of $CH_3NH_3PbI_3$ (MAPI) on the substrate. Deposition chamber operating pressure and gas flow is controlled by connecting a roughing vacuum pump (downstream) and an additional nitrogen valve in the third source tube (upstream). The completely assembled setup of the tool is presented in the photograph of Figure 1c.

The deposition process depends heavily on the following processing parameters: the flow rate of nitrogen at the source tube inlets, the temperature of the heated source tubes, the pressure of the system, and the substrate temperature. Since this is a large parameter space, for faster optimization, we implemented a fully coupled computational two-dimensional (2D) simulation of the momentum balance, the energy balance, and the mass balance to predict the deposition behavior of the system. We note that the physical properties (such as flux, volume, concentration, densities, etc.) are still treated three dimensionally. We extracted the required thermodynamic characteristics of MAI and PbI_2 from the literature,[24,25] which allowed the determination of the temperature-dependent equilibrium vapor pressure of the materials, needed for the sublimation rate calculations.[12,16] We constrained our experimental parameter space further by limiting the maximum operating temperature to 450 °C and the maximum pump displacement velocity to 6 ft^3/min (see Figure S2 for the pump displacement volume diagram).

To predict the deposition behavior with these constraints, we simulated the velocity field, the pressure map, the temperature, and the concentration maps within the VTD system at the steady state with COMSOL. The simulation was accomplished by applying the following parameters: PbI_2 source temperature of 450 °C and N_2 flow rate of 2000 SCCM, the MAI source temperature of 170 °C and N_2 flow rate of 1000 SCCM, the substrate temperature of 100 °C and the system pressure of 10 Torr. We plot the simulation results in Figure 2a,b, which are both divided into halves, as the results

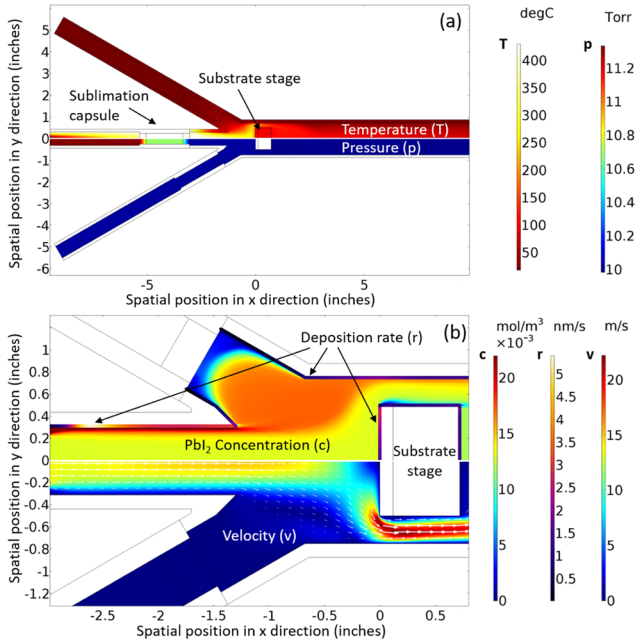

Figure 2. Simulated steady-state temperature (top half) and pressure (bottom half) map of the perovskite VTD tool (a). Simulated steady-state concentration map with deposition rate edge plots (top half) and velocity map with field arrows (bottom half) of the perovskite VTD tool (b).

are symmetrical. Figure 2a shows the temperature map in the top half and the pressure field in the bottom half. We notice from the plots that the temperature varies substantially throughout the geometry. The high flow rate influences the temperature distribution at the inlet of the PbI_2 source tube, which is wrapped with heating tape and well controlled. However, the source cell shows perfectly uniform heating at the constant maximum temperature of 450 °C, due to the slightly slowed downflow through the SiC filters. The pressure is almost constant at the controlled value of 10 Torr throughout the geometry and only undergoes a slight increase through the filters at steady state. Figure 2b shows the concentration map in the top half and the velocity map with field arrows in the bottom half.

We additionally calculated the deposition rate[14] on the chamber walls and on the substrate stage and plotted it as a color contour edge within the concentration map. We notice that the concentration map follows the shape of the velocity field. Hence, the distribution of the highly diluted PbI_2 vapor within the N_2 carrier gas is mostly driven by the directional laminar flow. Only at the boundary layers, it is driven by the concentration gradient, which is influenced by the temperature gradient. We find that the deposition rate (shown as color-mapped boundaries in Figure 2b) at the center of the substrate comes to roughly 1.5 nm/s and increases slightly at the edges, similar to the OVPD simulation results shown by others.[19] The equivalent modeling results of the MAI deposition are plotted in Figure S1. Due to the high vapor pressure of MAI, the deposition rate for a co-deposition is limited by the PbI_2 deposition and potentially the interdiffusion and crystal growth kinetics that have not yet been considered. When analyzing the

DOI: 10.1021/acsami.9b07651
ACS Appl. Mater. Interfaces 2019, 11, 32928−32936

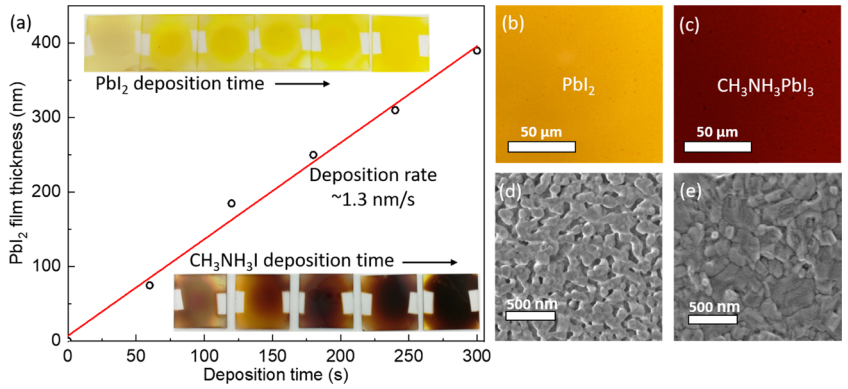

Figure 3. Photographs of VTD-deposited PbI_2 films with increasing deposition time (top inset) (a) and of sequentially VTD-deposited MAPI perovskite films with a set PbI_2 deposition time and increasing MAI deposition time (bottom inset) (a). The plot of PbI_2 film thickness dependent on VTD deposition time and linear fit to show the growth rate (a). Optical micrographs (b, c) and SEM images (d, e) of PbI_2 and MAPI perovskite films deposited sequentially with VTD.

deposition rate, we encounter very high parasitic deposition of the material within the part of the source tube after the source cell. The current design does not allow for heating the end of the center tube to higher temperatures. For an improved design, heating the reactor walls to the substrate stage should be considered to maximize material utilization and to accomplish higher deposition rates. In such a case, the substrate stage would have to be substantially cooled to keep the surface temperature low enough for efficient deposition. The results of this simulation should be used predominantly for qualitative trend analysis instead of exact quantitative predictions, as they were computed in simplified 2D space due to computation time limitations and lacking an exact sticking coefficient study for precise deposition rate analysis. Both are beyond the scope of this work.

Guided by the simulation results, we sequentially deposited perovskite films by first vapor-transporting PbI_2 onto the substrate and then subsequently exposing it to a transported vapor stream of MAI to form MAPI perovskite films. This deposition sequence allows us to adjust the right stoichiometric compositional combination of the materials by changing only the deposition times. To optimize the process and compare deposition rates with simulation results, we started with different deposition time durations for the two materials. After preheating the source tubes for at least 5 min (PbI_2) or 2 min (MAI) to allow for steady-state sublimation, we opened the nitrogen carrier gas valves for different deposition times. We show the appearance of the increasingly thicker PbI_2 films in the inset photographs of Figure 3a and plot their thicknesses, determined by a profilometer, as a function of the increasing deposition durations. The resulting linear growth behavior corresponds to a growth rate of 1.3 nm/s, which is about 10 times faster than demonstrations of thermally evaporated PbI_2 films.[26] We notice a difference between the increasing thickness of the deposited films toward the edge and the deposition rate profiles of the simulation. As the deposition rate is highly dependent on the boundary layer (velocity profile at the deposition surface), it is likely that our simplified 2D simulation does not lead to correct results of the velocity simulation between the round inner chamber walls and the quadratic substrate stage (visible in the corners of the substrates with VT-deposited films). Furthermore, it is plausible that the temperature of our substrates is not uniform, as assumed in the simulation, but hotter at the edges due to reduced heat distribution within the substrate stage. This would lead to a significantly reduced deposition rate, as the sticking coefficient has a strong dependence on temperature.[14] We decided to use a PbI_2 film thickness of ca. 200 nm, reached after 3 min of VTD, to convert to MAPI films. As discussed earlier, the PbI_2 deposition rate is the limiting process as the vapor pressure of MAI is substantially higher, which corresponds to a much faster deposition speed. The increased duration of MAI VTD is leading to films with initial PbI_2 excess and then gradually changing to more stoichiometrically balanced compositions and then to compositions with an excess of MAI. This coarse optimization process is displayed as a color change in the inset photographs of Figure 3a. We examined the morphology of the optimal VTD PbI_2 film and converted MAPI film by 50× magnified optical microscopy and scanning electron microscope (SEM) imaging of the surfaces. The resulting images of PbI_2 (b, d) and MAPI (c, e) are shown in Figure 3b–e. We find that the PbI_2 morphology appears to be porous with ca. 100 nm large islands, which could help to allow for enhanced MAPI conversion due to larger available surface area.[27,28] Consequently, the pin-hole free morphology of MAPI appears to have a good quality perovskite crystal grain size of roughly 200 nm. Hence, these films should allow for well-functioning absorber layers in perovskite solar cell devices with less trap probability within the grain boundaries.[29]

Sequentially depositing the precursor materials is not regarded as the fastest and, therefore, most scalable technique for the vapor-based perovskite fabrication. This is due to the conversion of PbI_2 to MAPI upon MAI exposure requiring an initial diffusion of the organic material to then convert to the perovskite crystal structure. Thick PbI_2 (>100 nm) films, required to make thick enough absorber layers to maximize charge carrier generation, require a longer time for the intercalation of MAI and conversion to perovskite.[30−32] One solution to this challenge is to deposit an alternating sequence of thin pairs of films that add up in thickness to the original thick film pair. Specifically, we deposited pairs of PbI_2 and MAI three times in a row. To compare the optical properties of the resulting films, we measured the UV−vis absorbance spectra of bare PbI_2 films that were deposited via VTD as well as a sequentially deposited layer of PbI_2 for 3 min and then vapor transport (VT) depositing MAI for 1 min and repeating the former procedure three times. Results shown in Figure 4a

DOI: 10.1021/acsami.9b07651
ACS Appl. Mater. Interfaces 2019, 11, 32928−32936

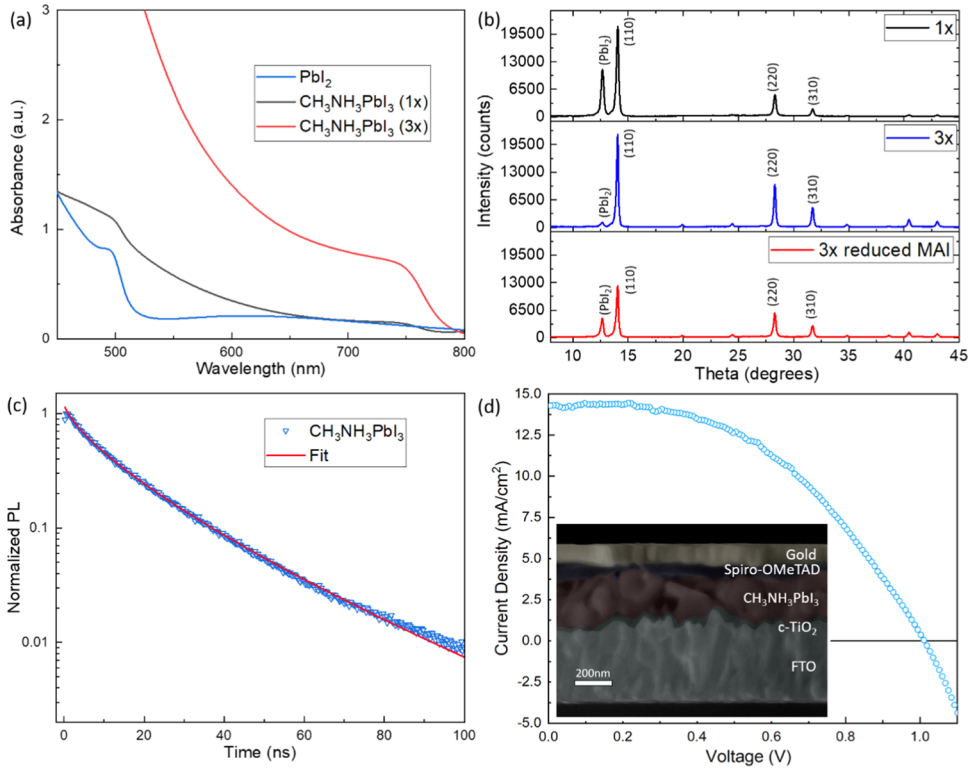

Figure 4. UV−vis absorbance spectra of PbI_2 films and MAPI films produced via one sequential VT deposition and three alternating sequential VT depositions (a). X-ray diffraction spectra of MAPI films produced via one sequential VT deposition and three alternating sequential VT depositions as well as three alternating sequential VT depositions with reduced MAI exposure (b). Plots of the time-resolved photoluminescence decay of VTD-deposited MAPI films with stretched exponential decay fit (c). Characteristic *JV* curve of the VT-deposited perovskite solar cell device under simulated AM 1.5 sunlight (d) with the cross-sectional SEM image of the device stack (inset).

demonstrate that the alternating sequential VTD technique leads to perovskite films that absorb significantly more light. The absorbance onset suggests a band-gap edge at a wavelength of 780 nm (corresponding to 1.59 eV), which is in accordance with the typical properties of MAPI films.[33] The VTD PbI_2 film shows a band-gap edge at 520 nm (corresponding to 2.39 eV), which is also in good agreement with other reports.[34] To analyze the detailed compositional changes in the different MAPI films, we measured the X-ray diffraction (XRD) patterns, as shown in Figure 4b. The three times alternated sequentially deposited perovskite films are more crystalline, as evidenced by the nearly complete diminishment of the lead iodide peak, which has a typical appearance at around 12−13° and the dominance of the MAPI perovskite peak at 14°.[35] A trial of four times alternated sequentially deposited perovskite films resulted in substantial excess of MAI on the surface, which lead to rapidly degrading films that could not be measured quickly enough. On an additional sample, we reduced the MAI deposition time slightly to see the effect in the XRD spectrum and find that the conversion to the perovskite phase is reduced, as determined by the decreased MAPI peak at 14° and the reappearing of the PbI_2 peak. Reassuring us of having reached a close to optimal condition[36] with the initial protocol of three times alternated sequential deposition.

Figure 4c plots the PL decays of a bare VTD MAPI film together with a fitted stretched exponential decay. We find that the average monomolecular carrier lifetime of our VTD $CH_3NH_3PbI_3$ perovskite film, determined with the exponential fit,[37] equals 10.3 ns. Although this is shorter than some results taken from films made via solution processing or special passivation,[38] it appears to match with published results from thermally evaporated films[32,37,39,40] without passivation that leads to well-working solar cell devices.

Above results indicate that VTD MAPI films have good optoelectronic properties and good morphology, which could lead to well-performing MAPI perovskite solar cells. To fabricate solar cells with VTD MAPI films, we start with fluorinated tin oxide (FTO)-coated glass on top of which a TiO_2 compact electron transporting layer is spin-coated and high-temperature-annealed. The VTD MAPI layer is then deposited and capped with a spin-coated spiro-OMeTAD hole-transporting layer and a thermally evaporated gold top contact. The device stack is shown in the inset cross-sectional SEM image of Figure 4d, with the *J*−*V* characterization under simulated AM 1.5 weighted sunlight plotted in Figure 4d. The functioning device has a PCE of 6.9%, coming from a short circuit current (J_{SC}) of 14.2 mA/cm^2, and a notably good open-circuit voltage (V_{OC}) of 1.01 V, indicating low recombination losses due to defect states or surface recombination. The fill factor (FF) of 0.48 is significantly lower than current high-performance results, and the shape of the curve indicates that there are substantial parasitic series resistances. Together with the relatively low J_{SC}, this indicates very inefficient charge extraction at one of the interfaces, which could be caused by an energy barrier from unoptimized perovskite compositions that still contain an excess of MAI or PbI_2 and need to be improved by further optimizing the growth conditions. Additionally, the low J_{SC} and FF could be an indication of a poor charge collection due to the

DOI: 10.1021/acsami.9b07651
ACS Appl. Mater. Interfaces 2019, 11, 32928−32936

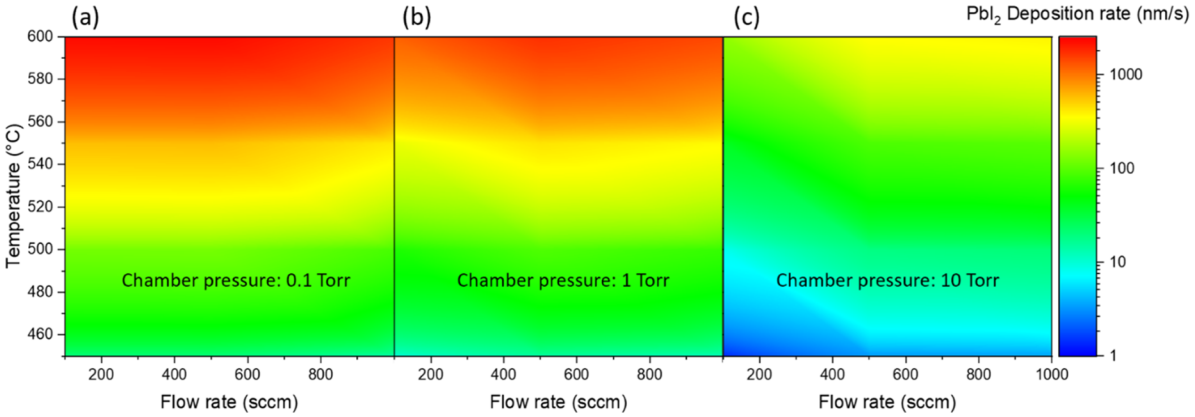

Figure 5. Simulated deposition rate as a function of source temperature and flow rate at chamber pressures of 0.1 Torr (a), 1 Torr (b), and 10 Torr (c).

nonoptimized thickness and material quality of the charge-transport layers. The device also displays a severe hysteresis effect[41,42] when comparing the *JV* curves from forward (J_{SC} to V_{OC}) and reverse (V_{OC} to J_{SC}) scan directions, as shown in Figure S3. The hysteresis is most likely an effect of the device architecture, as devices with MAPI as the absorber material and Li-doped spiro-OMeTAD as the hole-transporting material as well as TiO_2 as the electron transporting material have been demonstrated to display this effect.[43] We did not carry out any device stability studies, since devices that use this combination of materials are well known to be prone to quick degradation under ambient conditions.[44,45]

The scalability of the perovskite film fabrication with this novel VTD technique is the core focus of the present work. In the present implementation, the perovskite film-growth rate is dependent on the deposition rate of PbI_2 films. Therefore, to explore the deposition rate limits, we changed the processing conditions within our computational model to allow for optimized elevated source tube heating and chamber-wall heating to minimize the parasitic chamber-wall deposition during the film-growth process and maximize PbI_2 utilization. We show the effect that the processing parameters have on the deposition rate, by plotting the latter for varied source temperature and carrier gas flow rate at three different chamber pressures of 0.1 Torr (Figure 5a), 1 Torr (Figure 5b), and 10 Torr (Figure 5c). To check if the simulation can be appropriately carried out in the continuum flow regime even at lower pressures, we calculated the maximum Knudsen number and found it to never exceed 0.01 (see the Supporting Information). We find that by numerically optimizing the processing conditions, remarkably high deposition rates of over 2 μm/s are possible. The trends indicate that lowering the chamber pressure has a strong effect on increasing deposition rates, which can be explained by the increased sublimation rate at lower chamber pressures. Additionally, at high chamber pressures, increasing the carrier gas flow rate has a slightly positive effect on the deposition rate but a peak is visible at around 500 sccm for a chamber pressure of 1 Torr, in which too high rates again lead to a declining trend. This is not surprising as there are competing effects influencing the deposition rate, so although the higher flow rates above 500 sccm lead to an increased sublimation rate, it also dilutes the vapor and leads to smaller concentrations in the deposition regime. Finally, increasing the source temperature has a very strong effect on the deposition rate, easily explained by the exponential dependence of sublimation on temperature. The limit would be reached at the decomposition temperature of PbI_2.

It still needs to be proven that this technique can produce devices with equally high performances, as can be achieved as with other deposition methods. Additionally, some engineering challenges could emerge due to the need for precise process control systems, moderately high-temperature resistant components, and the need for a cooled substrate stage. However, the first experimental demonstrations and the results of the simulations are promising and open the doors for a remarkably fast deposition method for the active layers of perovskite solar cells.

EXPERIMENTAL SECTION

The glass substrates have been purchased from Pilkington Inc. with a coated fluorinated tin oxide (FTO) layer 15 Ω/sq. FTO was partially removed from the substrate via etching with zinc powder and 2 M HCl to create nonconductive stripes for later needed counter-electrode fabrication. The etched substrates were rinsed in deionized (DI) water and cleaned rigorously by brushing the Hellmanex solution with a toothbrush before rinsing again in a stream of DI water. N_2 was used to dry the substrates that were then subsequently rinsed in acetone and 2-propanol and then etched for 10 min in O_2 plasma. The n-type TiO_2 compact layer was formed by spin-coating a solution of 0.71 g titanium isopropoxide and 0.07 g of 2 M HCl in 8 ml of ethanol with 2000 rpm for 45 s and then annealed at 500 °C for 45 min.

The perovskite thin films were deposited with the custom-built tool, as demonstrated in the main text. The procedure started with the opening of the vacuum-tight system and the loading of the source materials. To keep the system clean and to support the reproducibility of the experiments, the material capsules including the metal parts and the SiC filter disks are cleaned thoroughly by immersion into dimethylsulfoxide (DMSO) and sonication for 5 min and then immersing and rinsing in isopropanol before drying with a stream of nitrogen and placement onto a 150 °C hotplate for 10 min. After assembly of the capsules, roughly 4 g of lead iodide (PbI_2) powder was loaded into one capsule and ca. 4 g of methylammonium iodide (MAI) powder was loaded into a second capsule. The source tubes of the VTD tool were cleaned by wiping the inside with DMSO-soaked cleanroom wipes that were pushed through the tube by a metal rod. The lead iodide capsule was then placed and pushed from the N_2 supply side into the middle source tube until it would not move further due to a tube narrowing at the very end. The MAI capsule was placed into the left source tube in the same way. The subsequent loading of the previously prepared substrate was performed by using a Kapton tape, which covers only a small area on the side of the

DOI: 10.1021/acsami.9b07651
ACS Appl. Mater. Interfaces 2019, 11, 32928−32936

substrate, to fasten it to the temperature-controlled metal stage. The tool was then closed up to allow for a roughing vacuum. The vacuum pump was turned on, and the system pressure reaches values close to 1×10^{-3} Torr after a couple of minutes. The vacuum pump is kept clean by using a cold trap that needs to be refilled with liquid nitrogen before every use. To keep the pressure of the system constant, the side N_2 inlet valve was opened, and the flow adjusted so that the chamber reaches a pressure of 10 Torr. Then, the circulation bath heater was turned on to 125 °C, and after a couple of minutes, the temperature-controlled substrate stage reached a measured temperature of ca. 100 °C. Without the use of the circulation bath heater, the substrate stage reaches a maximum temperature of 70 °C. Therefore, we actively heated the substrate during deposition. Subsequently, the middle PbI_2 source tube is heated to 450 °C, which is controlled by adjusting the power source of the resistive heating band and probing the temperature at the outside of the tube. Once the target temperature is reached, we wait 5 min for uniform, steady-state temperature distribution, and sublimation of the material before we turn on the N_2 source flow and simultaneously turning off the side inlet. The deposition flow is adjusted by sensing the pressure to equal exactly 10 Torr during deposition. The film thickness is controlled by timing the deposition time. For best results, a deposition time of 3×1 min for the PbI_2 deposition was used. After the PbI_2 deposition is finished, we turn off the N_2 source flow and simultaneously turning on the side N_2 flow to keep the pressure constant. At the same time, we turn off the power source for the heating band to decrease the temperature of the middle source tube. Then, we repeat the procedure in a similar manner with the MAI source tube. There we set the target source temperature to 210 °C and only wait 2 min to stabilize before starting with the deposition, which is also performed with adjusted N_2 flow to keep 10 Torr system pressure. The best results are achieved with a deposition time of 3×30 s. After turning off the source flow while turning on the side port flow and letting the temperature decrease, we wait for 15 min before turning off the vacuum pump and opening the system to remove the substrate.

For the fabrication of solar cell devices, the hole-transporting layer was deposited on top of the perovskite films by spin-coating a solution with 8.5 wt % spiro-OMeTAD in chlorobenzene and 30 mol % lithium bis(trifluoromethane-sulfonyl)imide and 80 mol % 4-*tert*-butylpyridine as additives, at 2000 rpm for 60 s in the dry air atmosphere. The sample was dried overnight in a light-sealed desiccator. Au (100 nm) was thermally evaporated on top of spiro-OMeTAD as the top electrode. The pressure was ca. 10^{-6} Torr and the evaporation rate was close to 0.1 nm/s.

For measuring the performance of the solar cells, simulated AM 1.5 sunlight was generated with a Newport solar simulator containing a Spectra Physics light source by Oriel Instruments. It was calibrated to give simulated AM 1.5, of 100 mW/cm^2 equivalent irradiance, using a calibrated silicon reference diode with a filter. The current−voltage curves were recorded with an Ossilla source measure unit T2002D. The solar cells were masked with a metal aperture defining the active area (0.2 cm^2) of the solar cells.

For the thickness measurements, we used a Bruker DXT Stylus Profilometer. The SEM images were taken with a Zeiss FESEM Ultra55 and the optical microscope images with a Nikon LV100 and a 50× Nikon (NA/WD: 0.80/1.0 mm) objective. We used a Rigaku SmartLab X-Ray Diffractometer to measure the X-ray diffraction patterns and a Cary 5000 UV−Vis−NIR Spectrophotometer for the UV−vis spectra. For the time-resolved photoluminescence measurements, a 405 nm Picoquant laser was used, with 100 s of 1 ps pulse width and a repetition rate of up to 80 MHz.

Additional details about the computational methods applied for the simulations is provided in the Supporting Information.

CONCLUSIONS

We present a novel vapor transport deposition method for perovskite thin films enabled by a custom-made multiple-source tool. Given the multicomponent nature of perovskite thin films, we found that a precise process control is needed for deposition of high-quality perovskite films. The choice of our processing parameters was guided by computational fluid dynamic simulations, which allowed for a determination of the effects of carrier gas flow and temperature, on the chamber pressure and vapor concentration, further allowing us to predict the perovskite film deposition profile on the substrate and chamber walls. In our experiments, we arrived at very high film deposition rates, surpassing 1 nm/s for PbI_2 and even faster for MAI. We demonstrated that the alternating sequential deposition can lead to perovskite thin films with high-quality morphology and crystallinity, similar to other deposition techniques that yield state-of-the-art films. The first solar cells containing perovskite photoactive films deposited with this novel technique already show a PCE of 6.9%. Finally, our computational simulations indicate that deposition rates on the order of micrometers per second should be possible by further optimizing this VTD process, which would benefit future scalable production of perovskite solar cells.

ASSOCIATED CONTENT

Supporting Information

The Supporting Information is available free of charge on the ACS Publications website at DOI: 10.1021/acsami.9b07651.

Computational methods, process simulation; domain governing equations used in the CFD simulations; calculation of the Knudsen number; vacuum pump displacement curve at varying pressure; characteristic *JV*-curve of VT deposited perovskite solar cell device (PDF)

AUTHOR INFORMATION

Corresponding Authors

*E-mail: maxhoer@mit.edu (M.T.H.).
*E-mail: bulovic@mit.edu (V.B.).

ORCID

Maximilian T. Hoerantner: 0000-0003-2297-3965
Haomiao Zhang: 0000-0001-7933-3155
Moungi G. Bawendi: 0000-0003-2220-4365
Klavs F. Jensen: 0000-0001-7192-580X

Notes

The authors declare no competing financial interest.

ACKNOWLEDGMENTS

The authors would like to thank Cedric Rolin (IMEC Belgium) and Kevin Bush (Swift Solar) for valuable discussions about the computational deposition model. Furthermore, we would like to thank Dane deQuilettes, Roberto Brenes, and Joel Jean for their help with the characterization of the thin films. This work was performed in part at the Center for Nanoscale Systems (CNS), a member of the National Nanotechnology Coordinated Infrastructure Network (NNCI), which is supported by the National Science Foundation under NSF award no. 1541959. CNS is part of Harvard University. This work was funded by the Tata Trust under the MIT GridEdge program. A.O. would like to acknowledge the support from the NSF under Grant No. 1605406 (EP/L000202).

REFERENCES

(1) Ono, L. K.; Qi, Y.; Liu, S. Progress toward Stable Lead Halide Perovskite Solar Cells. *Joule* **2018**, *2*, 1961−1990.

DOI: 10.1021/acsami.9b07651
ACS Appl. Mater. Interfaces 2019, 11, 32928−32936

(2) Noel, N. K.; Habisreutinger, S. N.; Wenger, B.; Klug, M. T.; Hörantner, M. T.; Johnston, M. B.; Nicholas, R. J.; Moore, D. T.; Snaith, H. J. A Low Viscosity, Low Boiling Point, Clean Solvent System for the Rapid Crystallisation of Highly Specular Perovskite Films. *Energy Environ. Sci.* **2017**, *10*, 145−152.
(3) Eperon, G. E.; Burlakov, V. M.; Docampo, P.; Goriely, A.; Snaith, H. J. Morphological Control for High Performance, Solution-Processed Planar Heterojunction Perovskite Solar Cells. *Adv. Funct. Mater.* **2014**, *24*, 151−157.
(4) Hörantner, M. T.; Nayak, P. K.; Mukhopadhyay, S.; Wojciechowski, K.; Beck, C.; McMeekin, D.; Kamino, B.; Eperon, G. E.; Snaith, H. J. Shunt-Blocking Layers for Semitransparent Perovskite Solar Cells. *Adv. Mater. Interfaces* **2016**, *3*, No. 1500837.
(5) Qiu, L.; Ono, L. K.; Qi, Y. Advances and Challenges to the Commercialization of Organic−inorganic Halide Perovskite Solar Cell Technology. *Mater. Today Energy* **2018**, *7*, 169−189.
(6) Kim, D. H.; Whitaker, J. B.; Li, Z.; van Hest, M. F. A. M.; Zhu, K. Outlook and Challenges of Perovskite Solar Cells toward Terawatt-Scale Photovoltaic Module Technology. *Joule* **2018**, *2*, 1437−1451.
(7) Liu, M.; Johnston, M. B.; Snaith, H. J. Efficient Planar Heterojunction Perovskite Solar Cells by Vapour Deposition. *Nature* **2013**, *501*, 395−398.
(8) Ávila, J.; Momblona, C.; Boix, P. P.; Sessolo, M.; Bolink, H. J. Vapor-Deposited Perovskites: The Route to High-Performance Solar Cell Production? *Joule* **2017**, *1*, 431−442.
(9) Momblona, C.; Gil-Escrig, L.; Bandiello, E.; Hutter, E. M.; Sessolo, M.; Lederer, K.; Blochwitz-Nimoth, J.; Bolink, H. J. Efficient Vacuum Deposited P-I-N and N-I-P Perovskite Solar Cells Employing Doped Charge Transport Layers. *Energy Environ. Sci.* **2016**, *9*, 3456−3463.
(10) Chang, N. L.; Ho-Baillie, A. W. Y.; Vak, D.; Gao, M.; Green, M. A.; Egan, R. J. Manufacturing Cost and Market Potential Analysis of Demonstrated Roll-to-Roll Perovskite Photovoltaic Cell Processes. *Sol. Energy Mater. Sol. Cells* **2018**, 314−324.
(11) Krebs, F. C.; Tromholt, T.; Jørgensen, M. Upscaling of Polymer Solar Cell Fabrication Using Full Roll-to-Roll Processing. *Nanoscale* **2010**, *2*, 873−886.
(12) Shtein, M. Organic Vapor Phase Deposition and Vapor Jet Printing for Electronic and Optoelectronic Device Applications. Doctoral Dissertation, Princeton University, 2004.
(13) Forrest, S. R. The Path to Ubiquitous and Low-Cost Organic Electronic Appliances on Plastic. *Nature* **2004**, *428*, 911−918.
(14) Kestner, J. M.; McElvain, S.; Kelly, S.; Ohno, T. R.; Woods, L. M.; Wolden, C. A. An Experimental and Modeling Analysis of Vapor Transport Deposition of Cadmium Telluride. *Sol. Energy Mater. Sol. Cells* **2004**, *83*, 55−65.
(15) Powell, R. C. *Research Leading to High Throughput Manufacturing of Thin-Film CdTe PV Modules: Annual Subcontract Report*, Sept 2004--Sept 2005, 2006.
(16) Shtein, M.; Gossenberger, H. F.; Benziger, J. B.; Forrest, S. R. Material Transport Regimes and Mechanisms for Growth of Molecular Organic Thin Films Using Low-Pressure Organic Vapor Phase Deposition. *J. Appl. Phys.* **2001**, *89*, 1470−1476.
(17) Burrows, P. E.; Forrest, S. R.; Sapochak, L. S.; Schwartz, J.; Fenter, P.; Buma, T.; Ban, V. S.; Forrest, J. L. Organic Vapor Phase Deposition: A New Method for the Growth of Organic Thin Films with Large Optical Non-Linearities. *J. Cryst. Growth* **1995**, *156*, 91−98.
(18) Baldo, M.; Deutsch, M.; Burrows, P.; Gossenberger, H.; Gerstenberg, M.; Ban, V.; Forrest, S. Organic Vapor Phase Deposition. *Adv. Mater.* **1998**, *10*, 1505−1514.
(19) Rolin, C.; Song, B.; Forrest, S. R. Mass Transport through the Carrier Gas Boundary Layer in Organic Vapor Phase Deposition. *Phys. Rev. Appl.* **2014**, *1*, No. 034002.
(20) Leyden, M. R.; Lee, M. V.; Raga, S. R.; Qi, Y. Large Formamidinium Lead Trihalide Perovskite Solar Cells Using Chemical Vapor Deposition with High Reproducibility and Tunable Chlorine Concentrations. *J. Mater. Chem. A* **2015**, *3*, 16097−16103.
(21) Jiang, Y.; Leyden, M. R.; Qiu, L.; Wang, S.; Ono, L. K.; Wu, Z.; Juarez-Perez, E. J.; Qi, Y. Large-Area Perovskite Solar Modules: Combination of Hybrid CVD and Cation Exchange for Upscaling Cs-Substituted Mixed Cation Perovskite Solar Cells with High Efficiency and Stability (Adv. Funct. Mater. 1/2018). *Adv. Funct. Mater.* **2018**, *28*, No. 1870007.
(22) Leyden, M. R.; Ono, L. K.; Raga, S. R.; Kato, Y.; Wang, S.; Qi, Y. High Performance Perovskite Solar Cells by Hybrid Chemical Vapor Deposition. *J. Mater. Chem. A* **2014**, *2*, 18742−18745.
(23) Tavakoli, M. M.; Gu, L.; Gao, Y.; Reckmeier, C.; He, J.; Rogach, A. L.; Yao, Y.; Fan, Z. Fabrication of Efficient Planar Perovskite Solar Cells Using a One-Step Chemical Vapor Deposition Method. *Sci. Rep.* **2015**, *5*, No. 14083.
(24) Dualeh, A.; Gao, P.; Seok, S. I.; Nazeeruddin, M. K.; Grätzel, M. Thermal Behavior of Methylammonium Lead-Trihalide Perovskite Photovoltaic Light Harvesters. *Chem. Mater.* **2014**, *26*, 6160−6164.
(25) Costa, J. C. S.; Azevedo, J.; Luís, M. N. B.; Mendes, A. On the Deposition of Lead Halide Perovskite Precursors by Physical Vapor Method. *J. Phys. Chem. C* **2017**, *121*, 2080−2087.
(26) Gil-Escrig, L.; Momblona, C.; La-Placa, M.-G.; Boix, P. P.; Sessolo, M.; Bolink, H. J. Vacuum Deposited Triple-Cation Mixed-Halide Perovskite Solar Cells. *Adv. Energy Mater.* **2018**, *8*, No. 1703506.
(27) Burschka, J.; Pellet, N.; Moon, S.-J.; Humphry-Baker, R.; Gao, P.; Nazeeruddin, M. K.; Grätzel, M. Sequential Deposition as a Route to High-Performance Perovskite-Sensitized Solar Cells. *Nature* **2013**, *499*, 316−319.
(28) Kim, Y. Y.; Park, E. Y.; Yang, T.-Y.; Noh, J. H.; Shin, T. J.; Jeon, N. J.; Seo, J. Fast Two-Step Deposition of Perovskite via Mediator Extraction Treatment for Large-Area, High-Performance Perovskite Solar Cells. *J. Mater. Chem. A* **2018**, *6*, 12447−12454.
(29) deQuilettes, D. W.; Vorpahl, S. M.; Stranks, S. D.; Nagaoka, H.; Eperon, G. E.; Ziffer, M. E.; Snaith, H. J.; Ginger, D. S. Solar Cells. Impact of Microstructure on Local Carrier Lifetime in Perovskite Solar Cells. *Science* **2015**, *348*, 683−686.
(30) Chen, Q.; Zhou, H.; Hong, Z.; Luo, S.; Duan, H.-S.; Wang, H.-H.; Liu, Y.; Li, G.; Yang, Y. Planar Heterojunction Perovskite Solar Cells via Vapor-Assisted Solution Process. *J. Am. Chem. Soc.* **2014**, *136*, 622−625.
(31) Chen, Y.; He, M.; Peng, J.; Sun, Y.; Liang, Z. Structure and Growth Control of Organic-Inorganic Halide Perovskites for Optoelectronics: From Polycrystalline Films to Single Crystals. *Adv. Sci.* **2016**, *3*, No. 1500392.
(32) Patel, J. B.; Milot, R. L.; Wright, A. D.; Herz, L. M.; Johnston, M. B. Formation Dynamics of CH3NH3PbI3 Perovskite Following Two-Step Layer Deposition. *J. Phys. Chem. Lett.* **2016**, *7*, 96−102.
(33) Lee, M. M.; Teuscher, J.; Miyasaka, T.; Murakami, T. N.; Snaith, H. J. Efficient Hybrid Solar Cells Based on Meso-Superstructured Organometal Halide Perovskites. *Science* **2012**, *338*, 643−647.
(34) Ahuja, R.; Arwin, H.; da Silva, A. F.; Persson, C.; Osorio-Guillén, J. M.; de Almeida, J. S.; Moyses Araujo, C.; Veje, E.; Veissid, N.; An, C. Y.; et al. Electronic and Optical Properties of Lead Iodide. *J. Appl. Phys.* **2002**, *92*, 7219−7224.
(35) Yin, J.; Cao, J.; He, X.; Yuan, S.; Sun, S.; Li, J.; Zheng, N.; Lin, L. Improved Stability of Perovskite Solar Cells in Ambient Air by Controlling the Mesoporous Layer. *J. Mater. Chem. A* **2015**, *3*, 16860−16866.
(36) Hsiao, S.-Y.; Lin, H.-L.; Lee, W.-H.; Tsai, W.-L.; Chiang, K.-M.; Liao, W.-Y.; Ren-Wu, C.-Z.; Chen, C.-Y.; Lin, H.-W. Efficient All-Vacuum Deposited Perovskite Solar Cells by Controlling Reagent Partial Pressure in High Vacuum. *Adv. Mater.* **2016**, *28*, 7013−7019.
(37) Stranks, S. D.; Eperon, G. E.; Grancini, G.; Menelaou, C.; Alcocer, M. J. P.; Leijtens, T.; Herz, L. M.; Petrozza, A.; Snaith, H. J. Electron-Hole Diffusion Lengths Exceeding 1 Micrometer in an Organometal Trihalide Perovskite Absorber. *Science* **2013**, *342*, 341−344.
(38) DeQuilettes, D. W.; Koch, S.; Burke, S.; Paranji, R. K.; Shropshire, A. J.; Ziffer, M. E.; Ginger, D. S. Photoluminescence

DOI: 10.1021/acsami.9b07651
ACS Appl. Mater. Interfaces 2019, 11, 32928−32936

Lifetimes Exceeding 8 μs and Quantum Yields Exceeding 30% in Hybrid Perovskite Thin Films by Ligand Passivation. *ACS Energy Lett.* **2016**, *1*, 438−444.
(39) Xing, G.; Mathews, N.; Sun, S.; Lim, S. S.; Lam, Y. M.; Grätzel, M.; Mhaisalkar, S.; Sum, T. C. Long-Range Balanced Electron- and Hole-Transport Lengths in Organic-Inorganic CH3NH3PbI3. *Science* **2013**, *342*, 344−347.
(40) Borchert, J.; Milot, R. L.; Patel, J. B.; Davies, C. L.; Wright, A. D.; Martínez Maestro, L.; Snaith, H. J.; Herz, L. M.; Johnston, M. B. Large-Area, Highly Uniform Evaporated Formamidinium Lead Triiodide Thin Films for Solar Cells. *ACS Energy Lett.* **2017**, *2*, 2799−2804.
(41) Snaith, H. J.; Abate, A.; Ball, J. M.; Eperon, G. E.; Leijtens, T.; Noel, N. K.; Stranks, S. D.; Wang, J. T.-W.; Wojciechowski, K.; Zhang, W. Anomalous Hysteresis in Perovskite Solar Cells. *J. Phys. Chem. Lett.* **2014**, *5*, 1511−1515.
(42) Tress, W.; Marinova, N.; Moehl, T.; Zakeeruddin, S. M.; Nazeeruddin, M. K.; Grätzel, M. Understanding the Rate-Dependent J–V Hysteresis, Slow Time Component, and Aging in CH 3 NH 3 PbI 3 Perovskite Solar Cells: The Role of a Compensated Electric Field. *Energy Environ. Sci.* **2015**, *8*, 995−1004.
(43) Wojciechowski, K.; Leijtens, T.; Siprova, S.; Schlueter, C.; Hörantner, M. T.; Wang, J. T.-W.; Li, C.-Z.; Jen, A. K.-Y.; Lee, T.-L.; Snaith, H. J. C60 as an Efficient N-Type Compact Layer in Perovskite Solar Cells. *J. Phys. Chem. Lett.* **2015**, *6*, 2399−2405.
(44) Pellaroque, A.; Noel, N. K.; Habisreutinger, S. N.; Zhang, Y.; Barlow, S.; Marder, S. R.; Snaith, H. J. Efficient and Stable Perovskite Solar Cells Using Molybdenum Tris (dithiolene) S as P-Dopants for Spiro-OMeTAD. *ACS Energy Lett.* **2017**, *2*, 2044−2050.
(45) Habisreutinger, S. N.; McMeekin, D. P.; Snaith, H. J.; Nicholas, R. J. Research Update: Strategies for Improving the Stability of Perovskite Solar Cells. *APL Mater.* **2016**, *4*, No. 091503.

DOI: 10.1021/acsami.9b07651
ACS Appl. Mater. Interfaces 2019, 11, 32928−32936